International Journal of Heat and Mass Transfer 52 (2009) 724–734

Contents lists available at ScienceDirect

International Journal of Heat and Mass Transfer

journal homepage: www.elsevier.com/locate/ijhmt

Numerical prediction of natural convection in vented cavities using restricted domain approach

S. Anil Lal *, C. Reji

Department of Mechanical Engineering, College of Engineering, Thiruvananthapuram 16, Kerala, India

ARTICLE INFO

Article history:
Received 30 December 2007
Received in revised form 28 March 2008
Available online 8 September 2008

Keywords:
Natural convection
Vented cavities
Restricted domain approach
SIMPLER algorithm
Upwind least square scheme

ABSTRACT

The present study reports the numerical simulation of natural convection heat transfer from an open square cavity with two side vents provided symmetrically on the side walls. The top wall which is maintained at a constant temperature (T_w), is the heat source for the cavity and the side walls are adiabatic. A restricted domain approach that predicts the regions of inflow, outflow and velocity distributions is employed. The applicability of two types of pressure boundary conditions at entry and exit regions are studied and compared. Non-linear coupled partial differential equations governing natural convection are solved on a structured non-uniform staggered grid using a second-order accurate upwind least square scheme for discretising the convection terms, central difference scheme for diffusion terms and SIMPLER algorithm for pressure–velocity decoupling. An in-house code is developed and is validated with the results of three classical natural convection problems. Simulations have been carried out for a wide range of thermal parameter, Rayleigh numbers ($10^4 \leqslant Ra \leqslant 10^8$), orientation of the cavity about horizontal ($0 \leqslant \delta \leqslant 180$) and geometrical parameter, vent ratio ($0.05 \leqslant \frac{D}{L} \leqslant 0.25$). The numerical simulation predicts the dimensionless mass flow rate through the cavity and variation of local Nusselt number over the hot wall. A correlation for average Nusselt number is developed in terms of Rayleigh number and angle of tilt of the cavity for $\frac{D}{L} \geqslant 0.1$.

1. Introduction

Natural convection in vented cavities is encountered in a variety of engineering applications such as electronic cooling devices, nuclear reactors, in buildings and so on. As is well known, for natural convection problems, the theoretical solution of governing equations in their full form is quite complex. The complexity multiplies due to uncertainty in the implementation of boundary conditions. Furthermore, the regions of entry and exit are not known in certain cases.

It is seen that the natural convection in vented cavities are solved using either an extended domain approach, to minimise the influence of boundary conditions in the solution or a domain restricted to the cavity itself (restricted domain). Zamora and Herandez [1] used an extended domain approach to study the influence of upstream conditions on a thermally optimum spacing of vertical plate array cooled by natural convection. Desrayaud and Lauriat [2] used an extended domain far from the opening due to hydrodynamic and thermal reasons and studied the natural convection in partially open enclosures with a conducting side wall. Kaiser et al. [3] reported correlation for Nusselt number in natural convection in vertical convergent channels at uniform wall temperature. They concluded that extension of the computational domain near the exit region did not produce any significant change in the results. Chan and Tien [4] compared the results of natural convection in a side open cavity, using both extended and restricted computational domains. In their study, a cold fluid flows over an adiabatic wall of the cavity before being heated up by a hot isothermal wall. The results obtained with restricted domain approach were almost same at high Rayleigh numbers, viz. $Ra = 10^6$ and $Ra = 10^9$. Khanafer and Vafai [5,6] have reported a set of appropriate boundary conditions at the entry and exit for natural convection in open enclosures.

Angirasa et al. [7] employed stream function-vorticity formulation and a restricted domain to simulate natural convection flow in a side open cavity. They assumed that the entry is irrotational and resultant velocity at the entry is normal to the side opening. Dehghan and Behnia [8] analysed natural convection in a top open discretely heated cavity using a restricted domain and stream function-vorticity formulation. The authors reported that, the entering fluid flows over an adiabatic wall of the cavity before getting heated up by the heat source. Polat and Bilgen [9] studied natural convection in side-open inclined cavities and reported that a computational domain restricted to the cavity with appropriate boundary conditions could produce results with very small

* Corresponding author. Tel.: +91 471 2515 584; mob: +91 9447007935; fax:+91 471 2598 370.
E-mail addresses: anillal65@hotmail.com (S. Anil Lal), rejic1979@gmail.com (C. Reji).

0017-9310/$ - see front matter © 2008 Elsevier Ltd. All rights reserved.
doi:10.1016/j.ijheatmasstransfer.2008.04.074

Nomenclature

D	height of the vent (m)
g	acceleration due to gravity (m s^{-2})
k	thermal conductivity (W m^{-1} K^{-1})
L	length of the square cavity (m)
$\dot{m}$	dimensionless mass flow rate
n	normal direction
$\mathbf{n}$	unit outward normal
Nu_x	local Nusselt number
$\overline{Nu}$	average Nusselt number
P	dimensionless fluid pressure
p	pressure (Pa)
Pr	Prandtl number
Ra	Rayleigh number
t	tangential direction
T	Temperature (K)
U	x component of dimensionless velocity
u	x component of velocity (m s^{-1})
$\mathbf{u}$	dimensionless velocity vector ($U_i + V_j$)
V	y component of dimensionless velocity
v	y component of velocity (m s^{-1})
X	dimensionless distance along x-coordinate
x	distance along x-coordinate (m)
Y	dimensionless distance along y-coordinate
y	distance along y-coordinate

Greek symbols

α	thermal diffusivity (m^2 s^{-1})
β	volume expansion coefficient (K^{-1})
θ	dimensionless temperature
ν	kinematic viscosity (m^2 s^{-1})
ρ	density (kg m^{-3})
ψ	dimensionless stream function
λ	slope of least square line
δ	angle of tilt of the cavity

Subscripts

∞	ambient
w	hot wall
0	stagnation
e	entering
l	leaving
i, j	unit vectors along X- and Y-directions

percentage deviation compared to extended computational domain. The angle of the cavity was varied from 0 to 90, thereby the geometry considered was changed from one with side open to top open. Later Bilgen and Oztop [11] studied the same problem by considering partial side opening using a restricted domain and primitive variable formulation. In their study the angle of cavity is varied from 0 to 120, thereby the cavity considered has a maximum 30° downward opening. Nateghi and Armfield [10] studied natural convection in inclined cavities for both unsteady and steady flows using restricted domain and primitive variable approach. In their work the cavity configuration is varied from side open to top open. It is evident that, for cases where fluid from the open space enters away from the cooling or heating walls, as those considered by Chan and Tien [4], Polat and Bilgen [9], Nateghi and Armfield [10], a restricted domain with appropriate boundary conditions is more effective as it results in substantial savings of CPU time and memory usage.

The foregoing discussion on the literature shows that natural convection from open cavities with multiple vents has not given much attention. The present work reports naturally induced fluid motion and heat transfer in a square cavity having a heated wall, side vents and an open edge, placed at different angular orientations. This is a case in which the fluid does not experience a sudden increase of temperature as soon as it enters the cavity and hence the use of restricted domain analysis is reasonable. A brief review of the literature on different types of boundary conditions for predicting natural convection in open cavities is discussed in this paper. Also, it reports the implementation of a second-order accurate scheme for the discretisation of convection terms, validation of the computer code and the prediction of flow and heat transfer characteristics of the problem considered.

2. Modelling

2.1. Geometry

The geometry of the cavity and the co-ordinate system are shown in Fig. 1. The cavity has an open edge, two side walls provided with openings (vents) and a heated wall at temperature T_w. The fluid outside the cavity is cold having temperature T_∞. The angle of inclination δ of the cavity with the horizontal is varied as $0 \leqslant \delta \leqslant 180$. At $\delta = 0$, the heated wall is horizontal and gets cooled from bottom. When $\delta = 90$, the heated wall becomes vertical and at $\delta = 180$, the heated wall becomes horizontal, but cooled from top.

2.2. Mathematical formulation

The non-dimensionalised set of governing equations expressed in primitive variables for a two-dimensional, incompressible flow with constant fluid properties and Boussinesq's approximation for buoyancy is given below:

$$\frac{\partial U}{\partial X} + \frac{\partial V}{\partial Y} = 0 \tag{1}$$

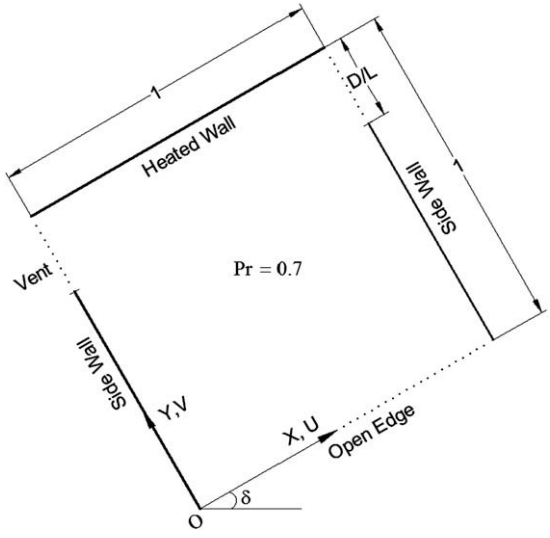

Fig. 1. Problem definition.

$$U\frac{\partial U}{\partial X}+V\frac{\partial U}{\partial Y}=-\frac{\partial P}{\partial X}+Pr\left(\frac{\partial^2 U}{\partial X^2}+\frac{\partial^2 U}{\partial Y^2}\right)+RaPr\theta\sin\delta \quad (2)$$

$$U\frac{\partial V}{\partial X}+V\frac{\partial V}{\partial Y}=-\frac{\partial P}{\partial Y}+Pr\left(\frac{\partial^2 V}{\partial X^2}+\frac{\partial^2 V}{\partial Y^2}\right)+RaPr\theta\cos\delta \quad (3)$$

$$U\frac{\partial \theta}{\partial X}+V\frac{\partial \theta}{\partial Y}=\left(\frac{\partial^2 \theta}{\partial X^2}+\frac{\partial^2 \theta}{\partial Y^2}\right) \quad (4)$$

where the dimensionless variable are defined as

$$X=\frac{x}{L},\quad Y=\frac{y}{L},\quad U=\frac{uL}{\alpha},\quad V=\frac{vL}{\alpha}$$
$$\theta=\frac{T-T_\infty}{T_w-T_\infty},\quad P=\frac{(p-p_\infty)L^2}{\rho\alpha^2}$$
$$Pr=\frac{\nu}{\alpha},\quad Ra=\frac{g\beta(T_w-T_\infty)L^3Pr}{\nu^2}$$

The dimensionless mass flow rate entering the cavity through an edge S is obtained by

$$\dot{m}_e=\int_S \max(-\mathbf{u}\cdot\mathbf{n},0)\,dS$$

where $\mathbf{u}$ is the dimensionless velocity vector at a point on S. Similarly, the dimensionless mass flow rate leaving the cavity through an edge S is

$$\dot{m}_l=\int_S \max(\mathbf{u}\cdot\mathbf{n},0)\,dS$$

The local Nusselt number is evaluated by:

$$Nu_X=\left.\frac{\partial\theta}{\partial Y}\right|_w$$

2.3. Boundary conditions

The solution of elliptic partial differential equations of natural convection flow in open cavities is found to be highly sensitive to boundary conditions at the entry and exit. A thorough examination of the different boundary conditions used by earlier investigators reveals that the differences are due to the boundary conditions for the tangential component of velocity at the entry and exit. Dehgam and Behnia [8], Nateghi and Armfield [10] and Angirasa et al. [7] used zero tangential component of velocity at the entry and exit. That is, the velocity at the entry and exit are taken normal to the edge. Singh and Venkateshan [12] investigated three different options for boundary conditions for velocity components at the inlet. Bilgen and Oztop [11] and Polat and Bilgen [9] have used the derivative of tangential component of velocity along the direction normal to the entry surface equal to zero as a boundary condition. All the investigators used boundary conditions for component of velocity normal to the opening by satisfying the continuity equation, ($\frac{\partial U}{\partial X}=-\frac{\partial V}{\partial Y}$). In this manner, the boundary condition for normal component of velocity varies corresponding to boundary conditions used for tangential component of velocity. Dehghan and Behnia [8], Angirasa [7], Singh and Venkateshan [12] and Balaji and Venkateshan [13] have used stream function vorticity formulation and they required boundary conditions for the vorticity at the inlet and exit. The boundary condition for vorticity is replaced by a pressure boundary condition in primitive variable formulation. It can be seen that the pressure boundary condition used are of two different types. Bilgen and Oztop [11] and Chan and Tien [4] used static pressure is equal to zero at inlet as well as exit as boundary condition. Zamora and Herandaz [1] and Evangellos et al. [14] equated static pressure at the exit and stagnation pressure at the inlet to zero gauge pressure, thereby there is a reduction in static pressure at the inlet corresponding to the magnitude of inlet velocity, according to Bernoulli's equation. These two types of boundary conditions for pressure are applied to a natural convection flow between two parallel heated walls. A comparison of the results obtained is given in Fig. 2.

Fig. 2(a) shows the velocity distribution when the static pressure at inlet and exit are set equal to zero. The velocity distribution at inlet and exit are found to be nearly the same, which means flow over the entire height is almost developed. However, as can be seen from Fig. 2(b), when the static pressure at the exit is equated to stagnation pressure at inlet, a uniform velocity distribution is obtained at the inlet. The flow then starts developing inside the passage. Thus the second type of boundary condition is more reasonable and adequate to simulate developing natural convection flow between parallel plates. In the present problem the second type of boundary condition is employed. All boundary conditions used in the present work are summarized in Table 1.

3. Numerical scheme

The transport equations are discretised on a structured non-uniform staggered grid using a second-order accurate upwind least square scheme (ULSS) for convection terms, central difference scheme for diffusion terms and solved by employing SIMPLER algorithm. ULSS [15] involves a pair of linear least square reconstruction of variable around each grid point, one each for x- and y-directions. Considering a grid point 'P', with E and W as neighbours in the x-direction as shown in Fig. 3. Let ϕ_W, ϕ_P and ϕ_E be the values of a general variable ϕ at W, P and E, respectively. A linear fit for ϕ around P assuming that the line passes through (x_P,ϕ_P) is given by

$$\phi=\phi_P+\lambda_P(x-x_p) \quad (5)$$

where the slope λ_P is obtained by least square fit considering the two other points (x_E,ϕ_E) and (x_W,ϕ_W). Thus we get

$$\lambda_P=\frac{(\phi_W-\phi_P)(x_W-x_P)+(\phi_E-\phi_P)(x_E-x_P)}{(x_E-x_P)^2+(x_W-x_P)^2} \quad (6)$$

The convective flux through a cell interface is approximated using the least square line on the upstream side of the cell face. For example, if the flow through e (denoted as F_e) is positive, then the least square line through P is used. On the other hand, the least square through E is used. Thus we get:

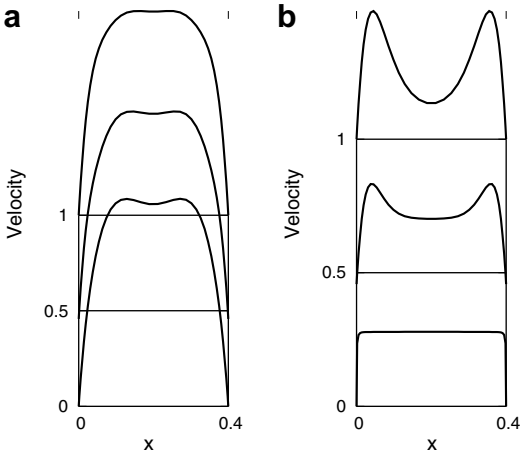

Fig. 2. Comparison of velocity distributions for different pressure boundary conditions. (a) Static pressure at the inlet and exit are equal to zero ($P_{inlet}=P_{exit}=0$). (b) Stagnation pressure at the inlet and static pressure at the exit are equated to zero ($P_{0(inlet)}=P_{exit}=0$).

Table 1
Boundary conditions

Side walls	$U = 0$, $V = 0$, $\frac{\partial P}{\partial X} = 0$, $\frac{\partial \theta}{\partial X} = 0$	
Heated wall	$U = 0$, $V = 0$, $\frac{\partial P}{\partial Y} = 0$, $\theta = 1$	
Openings	Pressure: $P_o = 0$ at entry, $P = 0$ at exit.	
	Left and right vents $\frac{\partial V}{\partial X} = 0$; $\frac{\partial U}{\partial X} = -\frac{\partial V}{\partial Y}$ $\theta = 0$ at entry; $\frac{\partial \theta}{\partial X} = 0$ at exit	Open edge $\frac{\partial U}{\partial Y} = 0$; $\frac{\partial V}{\partial Y} = -\frac{\partial U}{\partial X}$ $\theta = 0$ at entry; $\frac{\partial \theta}{\partial Y} = 0$ at exit

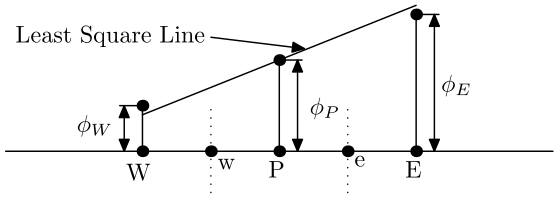

Fig. 3. A general grid point P, its neighbours E and W and a least square line.

$$F_e\phi_e = [\phi_P + \lambda_P(x_e - x_P)][\|(F_e, 0)\|] - [\phi_E + \lambda_E(x_e - x_E)][\|(-F_e, 0)\|]$$
$$= \overbrace{\phi_P[\|(F_e, 0)\|] - \phi_E[\|(-F_e, 0)\|]}^{\text{Term-1}}$$
$$+ \overbrace{[\|(F_e, 0)\|]\lambda_P(x_e - x_P) - [\|(F_e, 0)\|]\lambda_E(x_e - x_E)}^{\text{Term-2}} \quad (7)$$

where $[\|(A,B)\|]$ represents *maximum* of A and B.

The term-1 on the right-hand side of Eq. (7) is same as the classical first-order upwind scheme. In the present work, term-1 is added together with the coefficients of the system of equations. The term-2 is evaluated explicitly using the previous iteration values and is taken as an additional source term in the discretisation equation. The present scheme is basically an upwind scheme with second-order accuracy. The details of implementation of this scheme on unstructured hybrid grids is given in [15]. The vertical component of velocity at the inlet is evaluated such that the continuity equation in all the cells near the entry is exactly satisfied. The pressure at the cell centers of the inflow boundary cells is prescribed as a boundary condition. The under-relaxed discretisation equations are solved using a line-by-line iteration method with tri-diagonal matrix algorithm (TDMA) on each line. The under-relaxation factors for the solution of pressure and pressure correction are varied in the range 0.8–0.9. An under relaxation factor of 0.5 for the solution of velocity components has resulted stable solution on uniform grids, but the same has to be reduced up to 0.05 for getting a stable solution on non-uniform grids. However, the required under-relaxation factor depends on the degree of grid clustering near the walls.

4. Validation of numerical scheme

Three problems have been considered for validating the numerical scheme, viz.: (i) natural convection in a thermally driven enclosure [16], (ii) natural convection in a side open cavity [4], and (iii) natural convection from a vertical heated flat plate [18]. For the case of natural convection in a thermally driven enclosure, the results of the present work are found to be in very good agreement with the benchmark numerical solution by De Vahl Davis [16].

4.1. Natural convection in a side open cavity

Natural convection in a side open cavity is studied and the results are compared with a standard case reported by Chan and Tien [4]. The cavity has an open right wall and a heated left wall. The main difference between boundary conditions used in the present study and that in Chan and Tien [4] is the pressure boundary condition used at the entry and exit. In the present work, as discussed earlier, stagnation pressure of fluid at inlet and static pressure of the fluid at the exit are set equal to zero, where as Chan and Tien [4] have used static pressure at entry and exit, both equal to atmospheric pressure. Fig. 4 shows the streamline plots predicted by the present code for $Ra = 10^3$ and $Ra = 10^6$. The flow patterns predicted by the code is found to match well with the predictions of extended domain analysis by Chan and Tien [4]. A comparison of the dimensionless mass flow rate through the cavity and average Nusselt Number are tabulated in Table 2. As can be seen from the table, the percentage deviation in dimensionless mass flow rate for $Ra = 10^3$ is 13.58. The higher percentage deviation in dimensionless mass flow rate at $Ra = 10^3$ is expected due to low mass flow rate compared to that at high Ra. The predicted values of average Nusselt number agree well with those reported in [4].

Table 2
Comparison of dimensionless mass flow rate and $\overline{Nu}$ between present study and [4]

Ra	Present study		Chan and Tien [4] (extended domain)		Percentage deviation	
	$\dot{m}$	$\overline{Nu}$	$\dot{m}$	$\overline{Nu}$	$\dot{m}$	$\overline{Nu}$
10^3	2.29	1.28	2.65	1.33	13.58	3.76
10^6	44.77	15.16	47.40	15.00	5.55	1.07

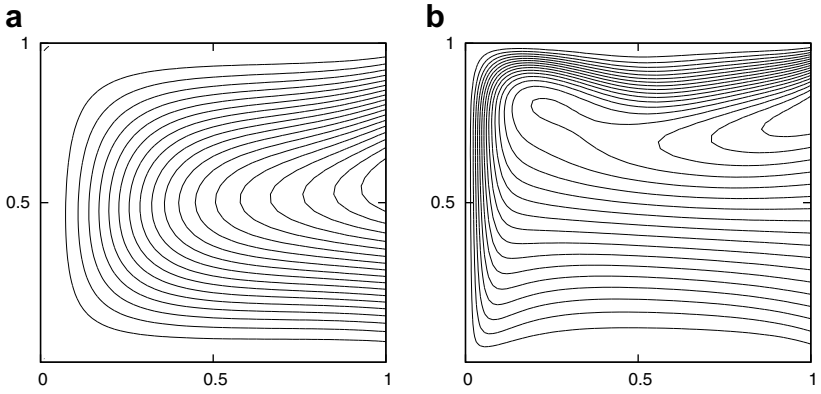

Fig. 4. Streamlines in a side open cavity. (a) $Ra = 10^3$ and (b) $Ra = 10^6$

4.2. Natural convection from a vertical heated flat plate

The present numerical scheme is used to simulate the naturally induced fluid motion and heat transfer from a heated vertical flat plate. Fig. 5 shows the computational domain and boundary conditions for the study. Air with $Pr = 0.7$ is used as the fluid. Numerical simulation has been carried out for $Ra = 10^5$, 10^6, 10^7 and 10^8. Fig. 6 shows a comparison of the predicted average Nusselt number with that calculated using correlation, $Nu = 0.68 + \frac{0.67Ra^{0.25}}{[1+(0.492/Pr)^{9/16}]^{4/9}}$ [17]. Excellent agreement of numerical prediction with those estimated using correlation highlights the adequacy of the present numerical scheme in simulating natural convection problems in open and vented cavities.

5. Results and discussion

5.1. Grid independence study

Grid independence tests have been carried out for three different orientations of the cavity, viz. $\delta = 0$, 90 and 180 for $Ra = 10^5$ and 10^6. For all the cases studied, D/L is kept constant at 0.2. The dimensionless mass flow rate and Nusselt number are the parameters considered for checking the convergence of results. The results are summarized in Table 3.

The grid is non-uniform with fine grids near the walls. The refinement near the walls is obtained using an exponential stretching function $\frac{d_i}{L} = 1 - \left[\frac{e^{\frac{s(N-i)}{N-1}}-1}{e^s-1}\right]$, where s is the stretching factor, d_i is the distance of ith point from the wall, 'N' is the total number of divisions and L is the total length. A value of $s = 2$ is used in the present work. A typical (80×80) non-uniform grid is shown in Fig. 7. Along X-direction, the grid contains refinement near the left and right walls and is applied uniformly from the center. Along Y-direction the regions above and below the bottom edge of the vents are considered differently. In the region above the vents, a non-uniform grid having refinement towards the hot wall is used. In the region below the vents, a uniform grid are used because any flow property variation in this direction is expected to be less compared to that occurring normal to the walls.

When $\delta = 0$, the heated wall is horizontal, at the top and is cooled from bottom and a grid independent result is obtained with a 30×30 grid. When $\delta = 90$, grid independent result is obtained on a 40×40 grid. But when $\delta = 180$, calculations were made using 100×100 grid also and the result was converged on an 80×80 grid. So this 80×80 grid has been used for the analysis of all the remaining cases.

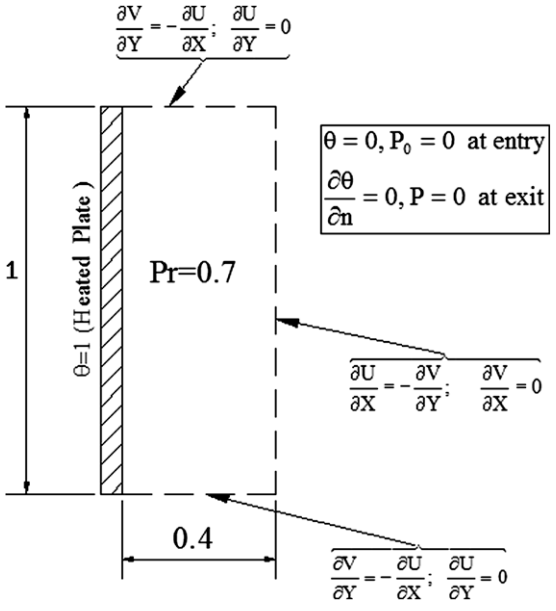

Fig. 5. Vertical heated flat plate – computational domain and boundary conditions.

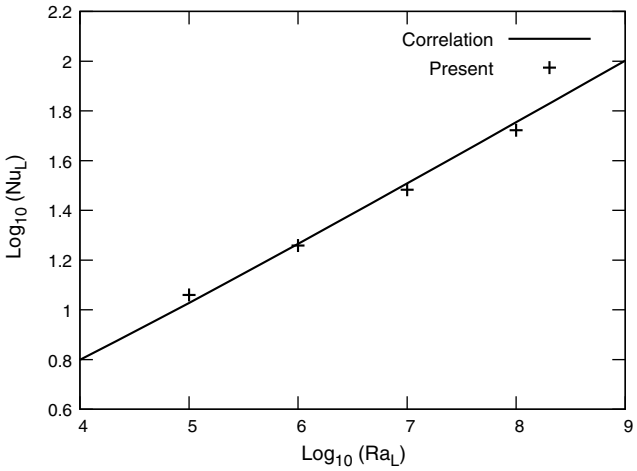

Fig. 6. Variation of Nusselt number with Rayleigh number over a heated vertical flat plate – comparison with correlation.

5.2. Effect of angle of tilt (δ)

Figs. 8–11 show the streamlines and isotherms inside the cavity for different orientations of the cavity, $\delta = 0$, 60, 150 and 180. For all values of δ, except $\delta = 180$, the major inflow of cold fluid takes place through the open edge of the cavity. Hot fluid leaves the cavity through the side vent located at the top. When $\delta = 0$, both the vents are at the same level and hence flow leaves the cavity symmetrically through the side vents. When $\delta = 180$, the side vents are located at the bottom and the cold fluid enters the cavity symmetrically through the vents. This fluid flows over the hot wall of the cavity, gets heated and rises up through the middle and leaves through the central portion of the open edge. Also, as can be seen from stream line plot, the cold fluid enters symmetrically through the left and right ends of the open edge. When $\delta = 150$, a small portion at the top end of the open edge of the cavity forms an exit for the hot fluid. For all angles other than $\delta = 150$ and 180 cold fluid enters through the entire length of the open edge.

Fig. 12 shows the variation of local Nusselt number over the hot wall for $\delta = 0$, 90, 150 and 180. At $\delta = 0$ and 180, the variations are symmetrical with respect to the center of heated plate ($X = 0.5$). Nusselt number is maximum at the ends and reduces towards the center. When $\delta = 90$, the fluid has the lowest temperature at $X = 0$, increases with X. Correspondingly the Nusselt number is maximum at $X = 0$ which reduces with increase of X. This is true because the flow starts developing from the leading edge. In the case of $\delta = 150$, local Nusselt number is maximum at $X = 0$, reduces with X, reaches a minimum at $X = 0.97$. In the remaining portion, there is a sharp increase of local Nusselt number. The reason for this increase beyond $X = 0.97$ is because flow enters through the vent at $X = 1$ nearby the hot wall (i.e., $Y = 1$) as indicated by the stream lines and isotherms in Fig. 10(a) and (b).

Fig. 13(a) and (b) shows the variations of dimensionless mass flow rate entering and leaving the cavity through different openings as a function of angle of tilt (δ). The total dimensionless mass flow rate entering the cavity increases with angle of tilt up to $\delta = 60$. In the range $60 \leqslant \delta \leqslant 144$, flow remains nearly constant with an average and standard deviation of 38.36 and 1.925, respectively. A very slight increase of angle from $\delta = 144$ to $\delta = 144.25$

Table 3
Mass flow rate and $\overline{Nu}$ for different grid sizes

Grid size	$\delta = 0$				$\delta = 90$				$\delta = 180$			
	$Ra = 10^5$		$Ra = 10^6$		$Ra = 10^5$		$Ra = 10^6$		$Ra = 10^5$		$Ra = 10^6$	
	$\dot{m}$	$\overline{Nu}$	$\dot{m}$	$\overline{Nu}$	$\dot{m}$	$\overline{Nu}$	$\dot{m}$	$\overline{Nu}$	$\dot{m}$	$\overline{Nu}$	$\dot{m}$	$\overline{Nu}$
30×30	13.33	6.54	23.63	10.35	20.02	10.87	40.54	17.64	39.00	11.33	81.43	15.68
40×40	13.39	6.54	23.65	10.33	19.98	11.08	40.21	17.81	39.10	11.60	80.23	16.50
50×50	13.42	6.54	23.68	10.32	19.96	11.24	40.04	17.91	39.33	12.13	78.15	16.73
60×60	13.44	6.53	23.69	10.30	19.94	11.37	40.02	17.98	39.37	12.34	77.24	17.09
80×80					19.91	11.56	40.01	18.01	39.43	12.52	76.80	17.22
100×100									39.46	12.58	76.78	17.24

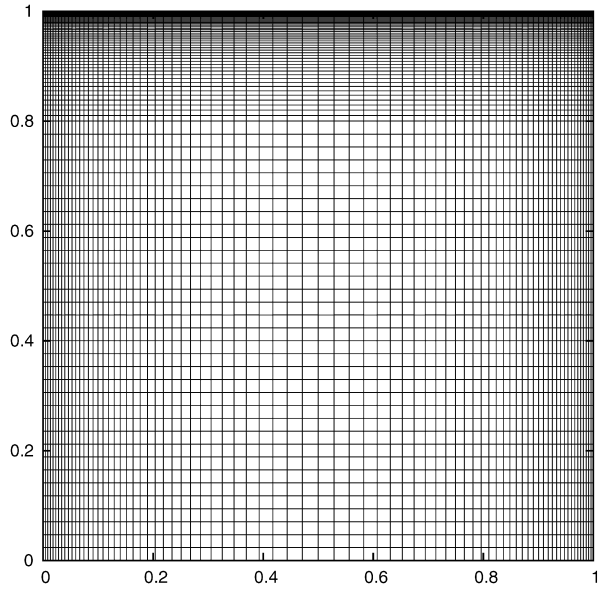

Fig. 7. An 80×80 grid pattern (vent ratio, $D/L = 0.2$).

causes a discontinuous increase of total flow from 35.9 to 38.7. It may be noted that, up to $\delta = 135$, the right wall is at the top most position and faces against the rising hot fluid. When δ is increased beyond 135, the open edge takes the top most position and fluid leaves through the top most end of the open edge for $\delta > 144.25$. When $\delta > 144.25$, flow enters the cavity through the right vent. Also there is a sharp increase in the mass flow entering through the right vent and mass flow leaving through the open edge. The total dimensionless mass flow rate through the cavity increases from 38.65 at $\delta = 144.25$ to 76.795 at $\delta = 180$. An almost 100% increase of flow in this range is attributed to the natural updraft occurring at these angles.

Fig. 14 shows the variation of average Nusselt number as a function of angle of tilt (δ). The average Nusselt number over the hot wall increases from 10.3 to 18.3 as δ increases from 0 to 90. With further increase of δ, Nusselt number is not found to increase much. The increased mass flow rate through the cavity beyond $\delta = 144$ does not cause a significant increase in the value of $\overline{Nu}$. The excess flow entering the cavity does not cause an increase of velocity within the boundary layer near the hot wall, but flows through the remaining portion of the cavity and leaves without absorbing much heat.

5.3. Effect of Rayleigh number

Effect of Rayleigh number on the heat transfer characteristics is described for a configuration of the cavity with $\delta = 90$ and $\frac{D}{L} = 0.2$. Fig. 15 shows the streamlines inside the cavity for $Ra = 10^4$ and 10^7. For $Ra = 10^4$, the cold fluid enters the cavity through the bottom vent as well as through the bottom region of the open edge. It then flows over the hot wall and leaves through vent on the top wall. Also, it can be seen that a portion of the flow entering the cavity through the open edge above $\frac{X}{L} = 0.5$ leaves through the top region of the open edge itself. As Ra increases, fluid enters through the entire height of the open edge of the cavity. It is found that the normal distance from the hot wall over which the fluid leaves the cavity through the right vent at top reduces with increase of Ra. In other words, stream lines converge towards the hot wall. Further, velocity within the boundary layer increases with increase of Ra. It can be seen from Fig. 15(b) that at $Ra = 10^7$, the hot fluid leaves through a fraction of the top vent close to the heated wall. The high exit velocity in this portion causes entrainment of cold fluid through the remaining portion of the top vent. The cold fluid penetrates up to a certain depth inside the cavity, gets heated and

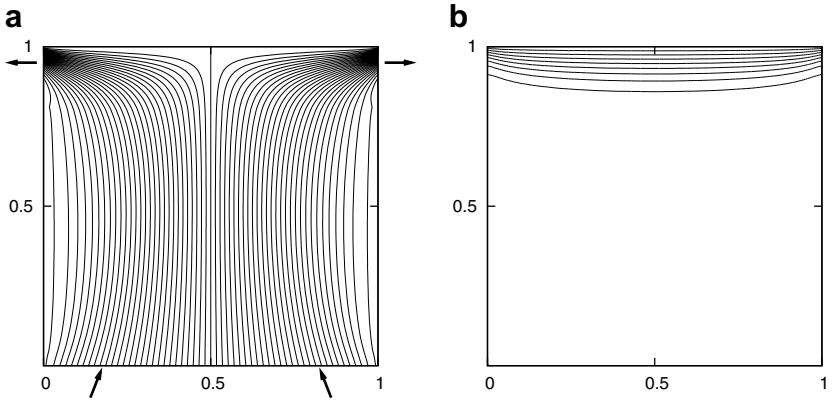

Fig. 8. Streamlines and isotherms for $Ra = 10^6$, $\delta = 0$, $\frac{D}{L} = 0.2$ ($\overline{Nu} = 10.304$, $\psi_{min} = -11.26$, $\psi_{max} = 11.26$).

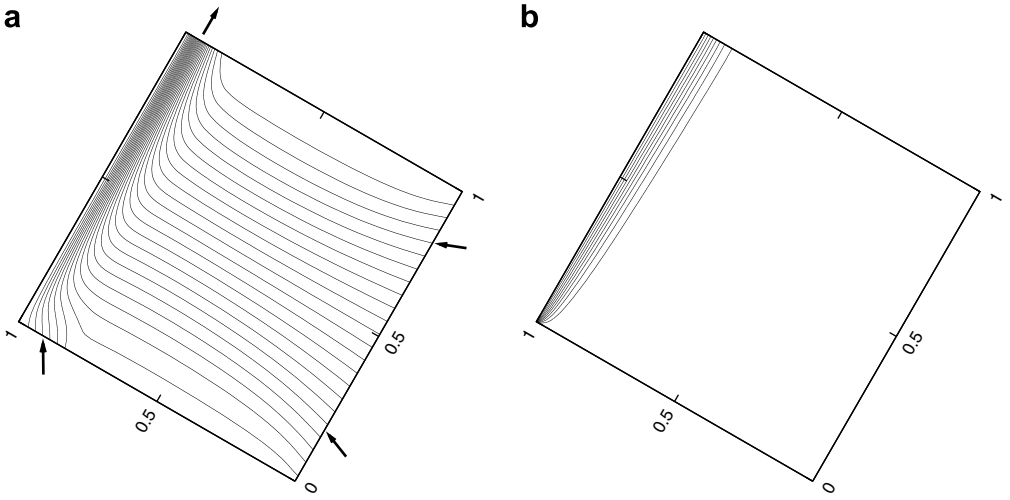

Fig. 9. Streamlines and isotherms for $Ra = 10^6$, $\delta = 60$, $\frac{D}{L} = 0.2$ ($\overline{Nu} = 17.214$, $\psi_{min} = -36.38$, $\psi_{max} = 0.0$).

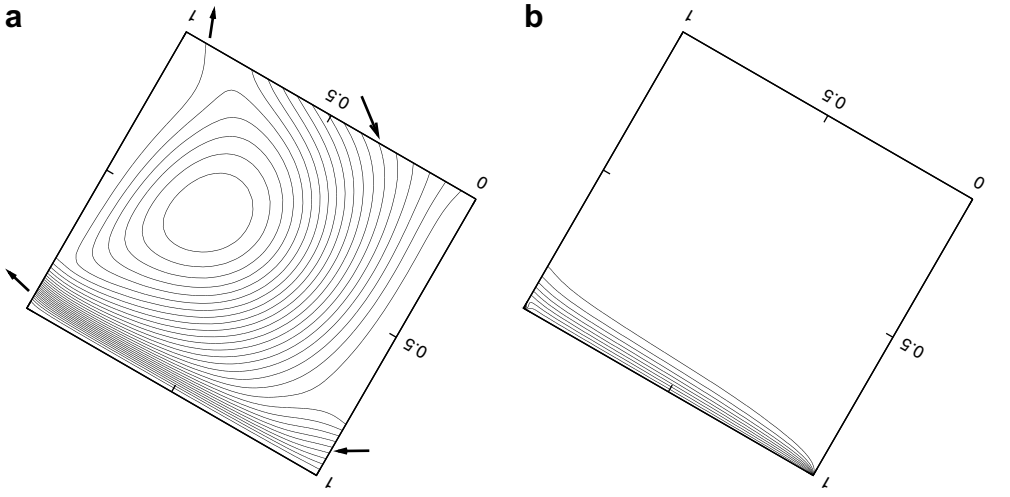

Fig. 10. Streamlines and isotherms for $Ra = 10^6$, $\delta = 150$, $\frac{D}{L} = 0.2$ ($\overline{Nu} = 17.951$, $\psi_{min} = -45.28$, $\psi_{max} = 0.07$).

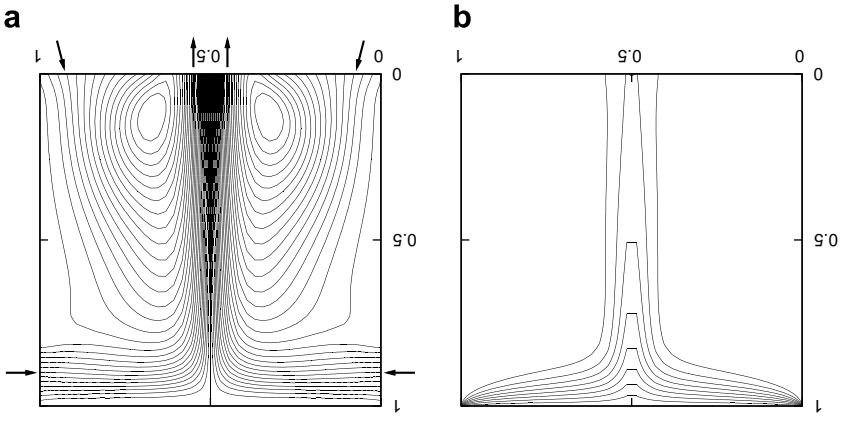

Fig. 11. Streamlines and isotherms for $Ra = 10^6$, $\delta = 180$, $\frac{D}{L} = 0.2$ ($\overline{Nu} = 17.219$, $\psi_{min} = -39.42$, $\psi_{max} = 39.42$).

mixes with the main exit flow. The depth of penetration of this cold fluid is found to be more for $Ra = 10^8$ than 10^7.

Fig. 16(a) and (b) shows the isotherms for $Ra = 10^4$ and 10^7. It is seen that the thickness of thermal boundary layer reduces with increase of Ra. At $Ra = 10^4$, as a result of redistribution of exit flow between the top vent and top end of the open edge as seen in Fig. 15(a), the isotherms in Fig. 16(a) are also redistributed over the same region. Both the ends of the top adiabatic wall experience

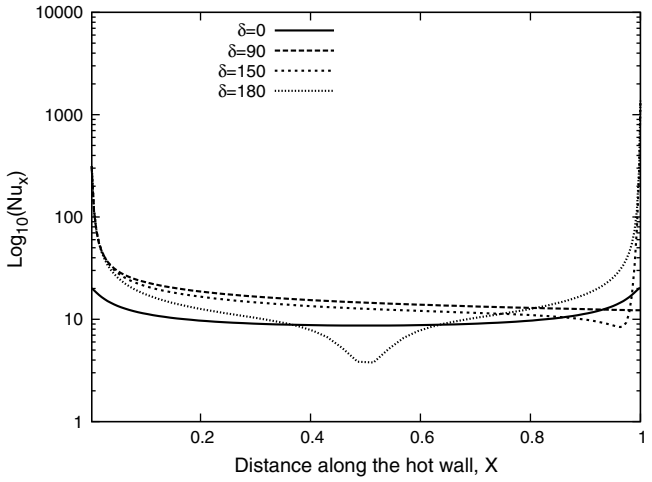

Fig. 12. Variation of local Nusselt number over the hot wall for various angles of tilt at $Ra = 10^6$.

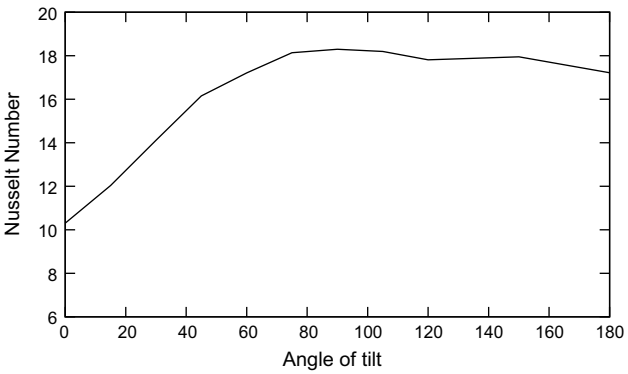

Fig. 14. Variation of average Nusselt number with δ for $Ra = 10^6$.

the temperature of hot fluid leaving the cavity and it becomes hot compared to the bottom adiabatic wall. As *Ra* increases the difference between temperatures of bottom and top adiabatic walls reduce. At $Ra = 10^7$, air inside the cavity is nearly at a uniform temperature with a very thin thermal boundary layer confined to the hot wall.

Fig. 17 shows the variation of local Nusselt number over the hot wall for $Ra = 10^4$, 10^5, 10^6, 10^7 and 10^8 for the configuration with $\delta = 90$. In all the cases, Nusselt number is maximum at the bottom edge of the hot wall ($X = 0$) as expected, reduces continuously indicating continuous heating of the fluid. Fig. 18 shows the variation of average Nusselt number over the hot wall and dimensionless mass flow rate through the cavity as a function of Rayleigh number. Both the parameters increase with increase in Rayleigh number, the rate of increase is more towards high values of Rayleigh number.

5.4. Effect of D/L

In this study, the vent ratio D/L is varied from 5% to 25% in steps of 5%, for three orientations of the cavity, viz. $\delta = 0$, 90 and 180. Fig. 19 shows the variation of dimensionless mass flow rate through the cavity. A clear reduction in dimensionless mass flow rate through the cavity for $D/L < 10\%$ is visible for all the cases except low Rayleigh number cases of $\delta = 90$. Fig. 20 shows the variation of average Nusselt number for $\delta = 0$, 90 and 180 at $Ra = 10^4$, 10^5, 10^6 and 10^7. For $\delta = 0$ and 180, the average Nusselt number is found to reduce as the vent ratio is reduced below 10%. When $\delta = 90$, Nusselt number is found to be independent of D/L up to $D/L = 5\%$. The reason for reduction in Nusselt number for vent ratios below $D/L = 10\%$ at $\delta = 0$ and 180 is due to the reduction of dimensionless mass flow rate. However, in the case of $\delta = 90$, the hydrodynamic boundary layer is very thin and the outgoing flow is unaffected by the restricted vent passage. In this case, the average Nusselt number is found to be independent of D/L up to 5%.

5.5. Nusselt number correlation

In order to develop a correlation for Nu with *Ra* and δ as parameters, Rayleigh number and δ are varied in the range $0 \leqslant Ra \leqslant 10^8$ and $0 \leqslant \delta \leqslant 180$, respectively. But for configuration with $\delta = 180$, the case of $Ra = 10^8$ is omitted as the flow in this case is turbulent. Fig. 21 shows the variation of average Nusselt number as a function of Rayleigh number for different values of δ. It is clear from the figure that the average Nusselt number increases with increase of δ, up to $\delta = 60$, the rate of increase of $\overline{Nu}$ reduces as δ increases from 30 to 60. For $Ra > 10^5$, the orientation $\delta = 90$ is found to have the maximum Nusselt number. For $\delta = 60$, 90 and 120, all the Nusselt number curves are very close to each other, indicating that variation of δ in this range does not cause much variation in $\overline{Nu}$. Nusselt number curves of $\delta = 120$ and $\delta = 150$ found to show slight variations on either sides of $Ra = 10^6$. Between $\delta = 150$ and 180, the Nusselt number does not vary much. For all values of Rayleigh number, the dependence of Nusselt number on angle of tilt, δ is found to be significant only in the range $0 \leqslant \delta \leqslant 60$. It is also found that for $D/L > 10\%$, the heat transfer characteristics through the cavity

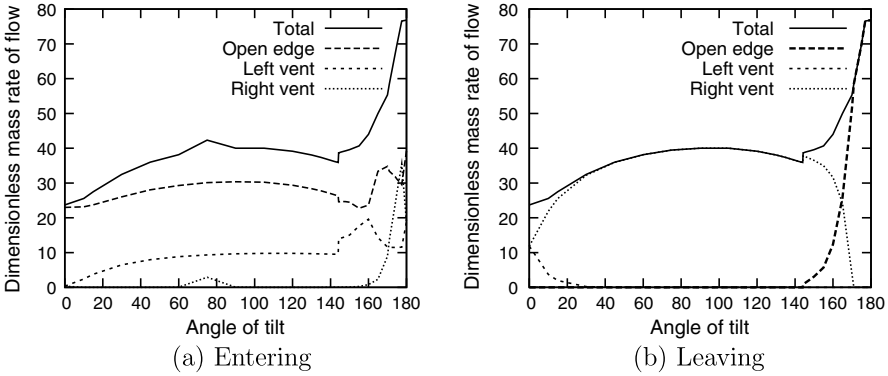

Fig. 13. Variation of dimensionless mass flow rate with δ for $Ra = 10^6$.

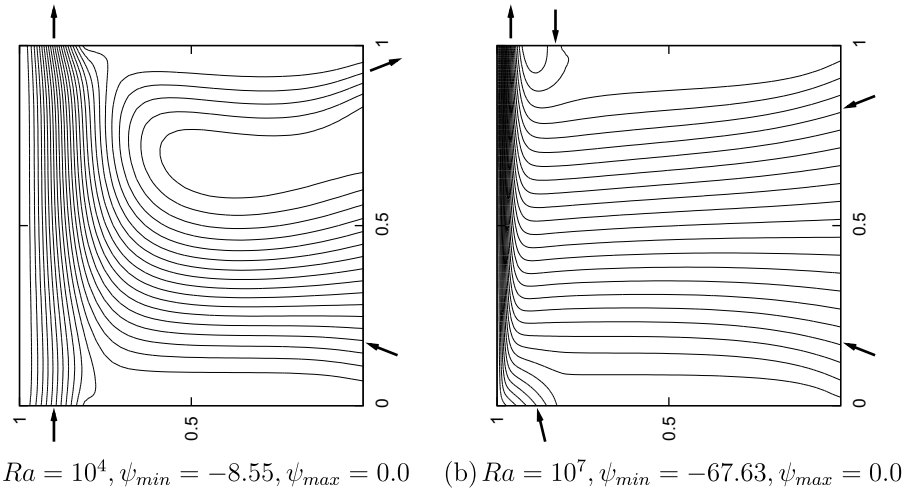

(a) $Ra = 10^4, \psi_{min} = -8.55, \psi_{max} = 0.0$ (b) $Ra = 10^7, \psi_{min} = -67.63, \psi_{max} = 0.0$

Fig. 15. Streamlines at various Rayleigh numbers (δ = 90 and $\frac{D}{L} = 0.2$).

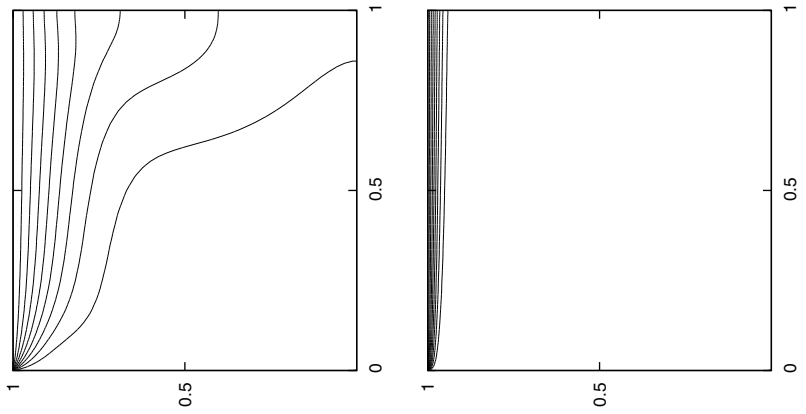

(a) $Ra = 10^4$ (b) $Ra = 10^7$

Fig. 16. Isotherms at various Rayleigh numbers (δ = 90 and $\frac{D}{L} = 0.2$).

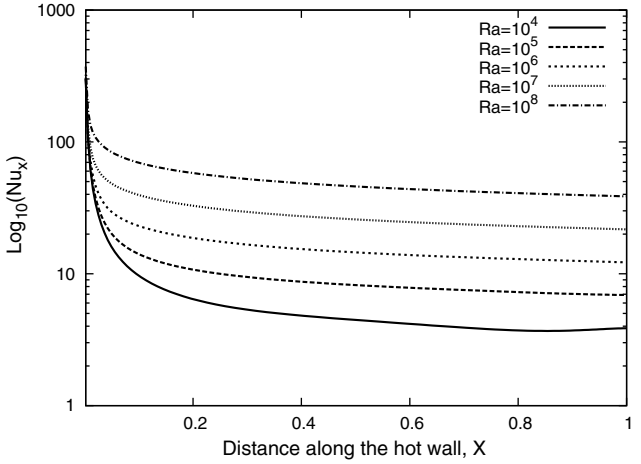

Fig. 17. Variation of local Nusselt number over the hot wall for different values of *Ra* at δ = 90.

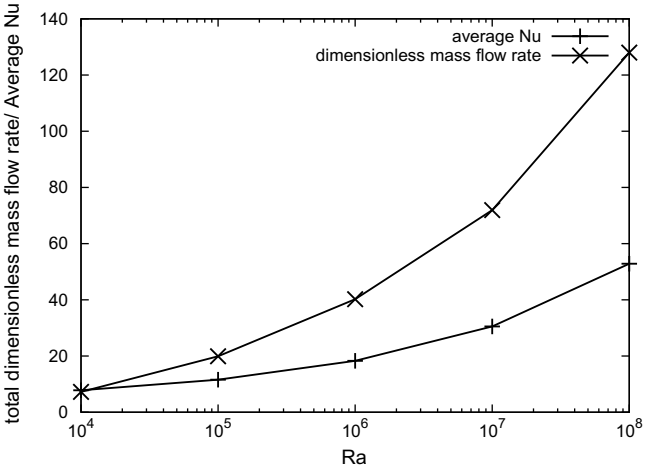

Fig. 18. Variation of average Nusselt number and dimensionless mass flow rate with Rayleigh number for δ = 90 and $\frac{D}{L} = 0.2$.

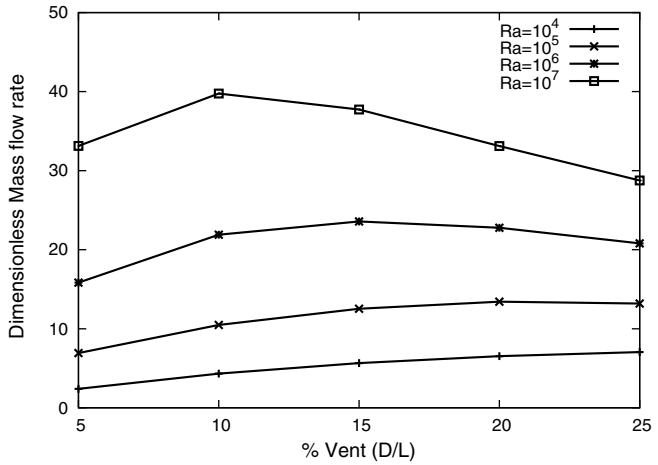

(a) $\delta = 0$

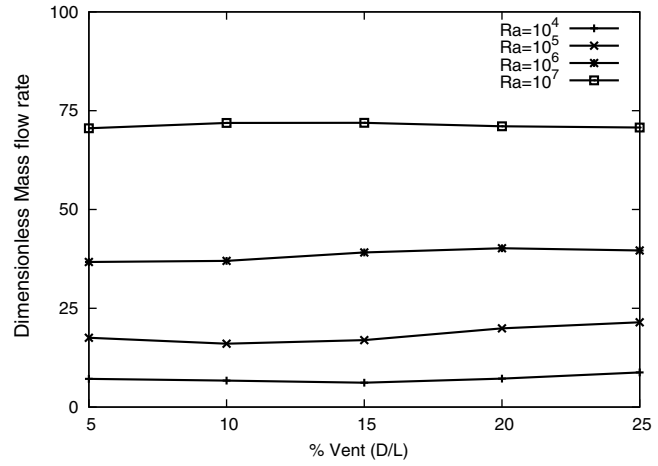

(b) $\delta = 90$

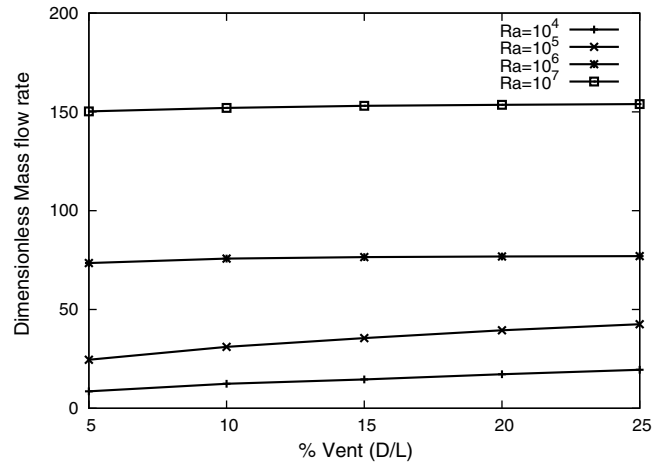

(c) $\delta = 180$

Fig. 19. Variation of dimensionless mass flow rate with D/L for different orientations of the cavity, δ.

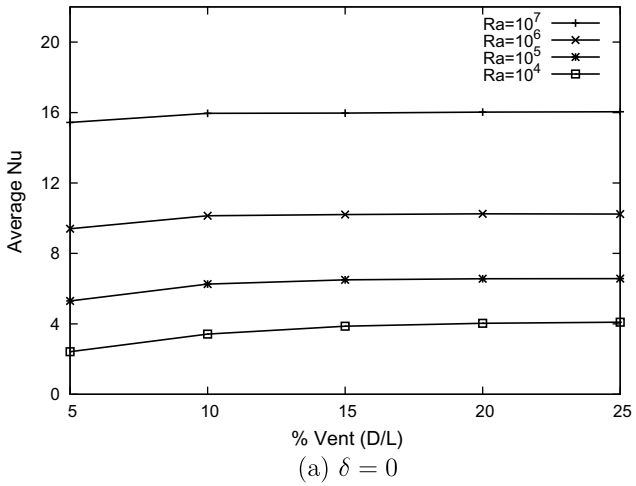

(a) $\delta = 0$

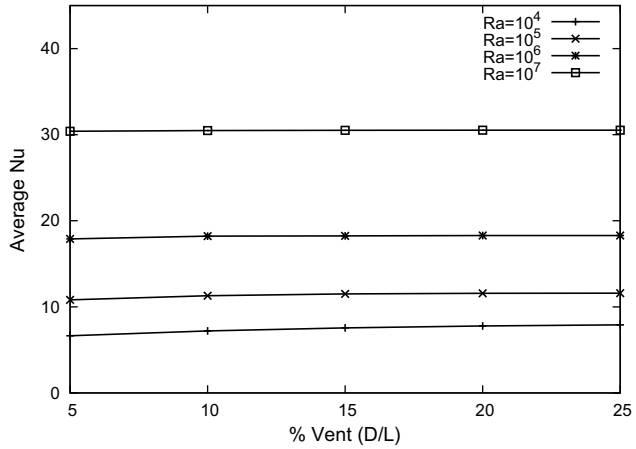

(b) $\delta = 90$

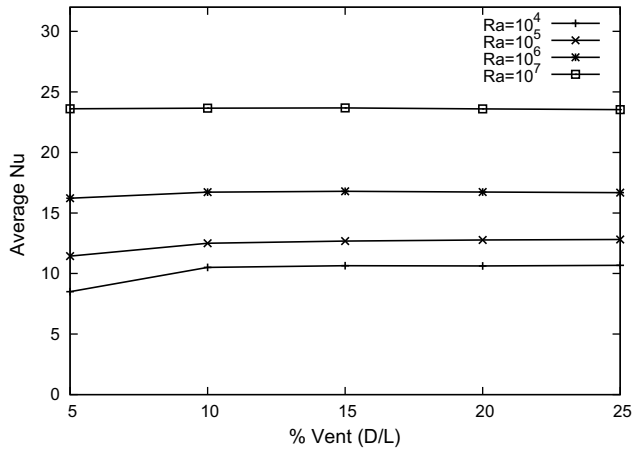

(c) $\delta = 180$

Fig. 20. Variation of average Nusselt number with D/L for different orientations of the cavity, δ.

is independent of D/L. Therefore, in the present work a four part correlation for Nusselt number is obtained as a function of angle of tilt of the cavity, δ and Rayleigh number for $10^4 \leqslant Ra \leqslant 10^8$, $0 \leqslant \delta \leqslant 180$, $D/L \geqslant 0.1$ and $Pr = 0.7$

$$\overline{Nu} = \begin{cases} 0.95Ra^{0.19}(\cos\delta)^{-0.76} & \text{for } 0 \leqslant \delta < 60 \\ 1.58Ra^{0.19} & \text{for } 60 \leqslant \delta < 120 \\ 1.31Ra^{0.19}(\cos(\pi+\delta))^{0.05} & \text{for } 120 \leqslant \delta < 150 \\ 1.23Ra^{0.19} & \text{for } 150 \leqslant \delta \leqslant 180 \end{cases}$$

The correlation coefficient of fit obtained is 0.9725.

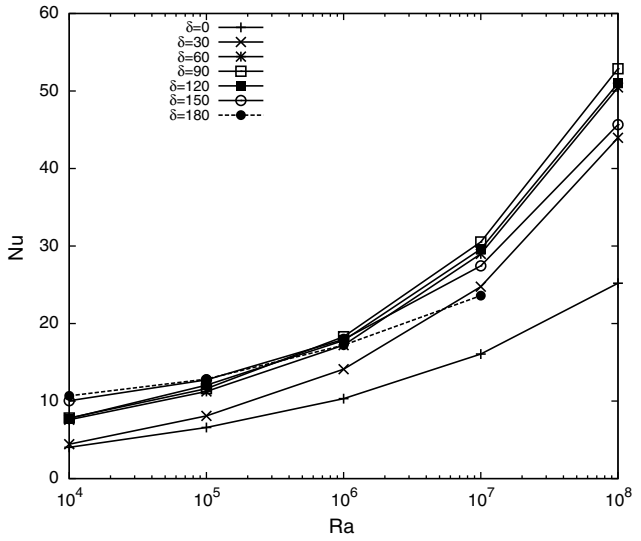

Fig. 21. Variation of $\overline{Nu}$ with Rayleigh Number for different values of δ with $\frac{D}{L} = 0.2$.

6. Conclusion

A restricted domain approach for the numerical simulation of natural convection flow and heat transfer in vented/open cavities is reported. A pressure boundary condition with stagnation pressure at inlet and static pressure at exit are equated to atmospheric pressure and a second-order accurate least square upwind scheme for the discretisation of convection terms are used for the numerical prediction. The efficacy of the numerical scheme is established with the results of three classical natural convection problems. The excellent agreement of the present numerical prediction with those reported in the literature highlights adequacy of the present numerical scheme.

In the case of natural convection in vented cavities with $Ra = 10^6$ and $\frac{D}{L} = 0.2$, the dimensionless mass flow rate through the cavity increases with increase of angle of tilt up to $\delta = 90$, it remains approximately same up to $\delta = 144$ and a drastic increase of mass flow rate is obtained at $\delta > 144$. Mass flow rate through the cavity is maximum for $\delta = 180$ and is attributed to updraft in the chimney like configuration. The excess flow through the cavity at $\delta = 180$ does not contribute to heat transfer when compared to $\delta = 90$. Thermal and hydrodynamic boundary layers over the heated wall become thin with increase of *Ra*. Maximum velocity in the boundary layer increases with increase of *Ra*. Reduction of vent ratio below $\frac{D}{L} = 0.1$ causes a restriction to the fluid flowing through side vents and results in reduction of Nusselt number. The average Nusselt number is found to be a strong function of angle of tilt of the cavity up to $\delta = 60$. For higher angles, average Nusselt number is found to be independent of angle of tilt or it is a very weak function of angle of tilt. For $Ra > 10^5$, the orientation with $\delta = 90$ is found to have the highest average Nusselt number. A correlation for average Nusselt number in terms of *Ra* and δ for $10^4 \leqslant Ra \leqslant 10^8$, $0 \leqslant \delta \leqslant 180$, $\frac{D}{L} \geqslant 0.1$ and $Pr = 0.7$ having a correlation coefficient 0.9725 is obtained.

References

[1] B. Zamora, J. Herandez, Influence of upstream conduction on the thermally optimum spacing of isothermal, natural convection-cooled vertical plate arrays, Int. Commun. Heat Mass Transfer 28 (2001) 201–210.
[2] G. Desrayaud, G. Lauriat, A numerical study of natural convection in partially open enclosures with a conducting side wall, J. Heat Transfer 126 (2004) 76–83.
[3] A.S. Kaiser, B. Zamora, A. Viedma, Correlation for Nusselt number in natural convection in vertical convergent channels at uniform wall temperature by a numerical investigation, Int. J. Heat Fluid Flow 25 (2004) 671–682.
[4] Y.L. Chan, C.L. Tien, A numerical study of two-dimensional laminar natural convection in shallow open cavities, Int. J. Heat Mass Transfer 28 (1985) 603–612.
[5] K. Khanafer, K. Vafai, Buoyancy-driven flows and heat transfer in open-ended enclosures: elimination of the extended boundaries, Int. J. Heat Mass Transfer 43 (2000) 2329–2344.
[6] K. Khanafer, K. Vafai, Effective boundary conditions for buoyancy-driven flows and heat transfer in fully open-ended two-dimensional enclosures, Int. J. Heat Mass Transfer 45 (2002) 2527–2538.
[7] D. Angirasa, M.J.B.M. Pourquie, F.T.M. Nieuwstatadt, Numerical study of transient and steady laminar buoyancy-driven flows and heat transfer in a square open cavity, Numer. Heat Transfer 22 (1992) 223–239.
[8] A.A. Dehghan, M. Behnia, Combined natural convection–conduction and radiation heat transfer in a discretely heated open cavity, J. Heat Transfer 118 (1996) 56–64.
[9] O. Polat, E. Bilgen, Conjugate heat transfer in inclined open shallow cavities, Int. J. Heat Mass Transfer 46 (2003) 1563–1573.
[10] M. Nateghi, S.W. Armfield, Natural convection flow of air in an inclined open cavity, ANZIAM J. 45 (E) (2004) C870–C890.
[11] E. Bilgen, H. Oztop, Natural convection heat transfer in partially open inclined square cavities, Int. J. Heat Mass Transfer 48 (2005) 1470–1479.
[12] S.N. Singh, S.P. Venkateshan, Numerical study of natural convection with surface radiation in side-vented open cavities, Int. J. Therm. Sci. 43 (2004) 865–876.
[13] C. Balaji, S.P. Venkateshan, Interaction of radiation with free convection in an open cavity, Int. J. Heat Fluid Flow 15 (4) (1994) 317.
[14] Bacharoudis Evangellos, Michalis Gr. Vrachopoulos, Maria K. Koukou, Dionysios Margaris, Andronikos E. Filios, Stamatis A. Mavrommatis, Study of the natural convection phenomena inside a wall solar chimney with one wall adiabatic and one wall under a heat flux, Appl. Therm. Eng. 27 (2007) 2266–2275.
[15] Marcelo H. Kobayashi, Jose M.C. Pereira, Jose C.F. Pereira, A conservative finite-volume second-order accurate projection method on hybrid unstructured grids, J. Comput. Phys. 150 (1999) 40–75.
[16] G. De Vahl Davis, Natural convection of air in a square cavity: a bench mark numerical solution, Int. J. Numer. Meth. Fluids 3 (1983) 249–264.
[17] S.W. Churchil, H.H.S. Chu, Correlating equations for laminar and turbulent free convection from a vertical plate, Int. J. Heat Mass Transfer 18 (1975) 1323.
[18] Frank P. Incropera, David P. DeWit, Fundamentals of Heat and Mass Transfer, fifth ed., Wiley, New York, 2002.